AIAA JOURNAL
Vol. 44, No. 9, September 2006

Scattering of Sound by Liner Splices: A Kirchhoff Model with Numerical Verification

Brian J. Tester* and Christopher J. Powles†
University of Southampton, Southampton, SO17 1BJ England, United Kingdom
and
Nicholas J. Baker‡ and Andrew J. Kempton§
Rolls–Royce plc, Derby, DE24 8BJ England, United Kingdom

DOI: 10.2514/1.17678

Variations in the impedance of the acoustic liners in aeroengine intake ducts occur due to the presence of acoustically hard splices, which lead to scattering of the incident fan tone noise into a large number of azimuthal modes, and can significantly reduce the effectiveness of the liner. Currently available computational aeroacoustic packages are capable of modeling the scattering, but are generally impractical for direct application to liner optimization design studies, because they require a substantial quantity of CPU time. A Kirchhoff approximation is applied to a geometry of practical interest, and the predicted field is compared with that computed using a commercially available computational aeroacoustic package. The analytical and computational results are in good agreement for cases both with and without mean flow. A striking result is that the modal power in most of the forward-scattered modes is almost equal, except for a small number of modes close to the rotor-alone mode. The analytical model is found to be accurate for a physically useful combination of parameters, and provides both a method for rapid evaluation of the scattering, and a physical understanding of the process.

Nomenclature

A	=	area of cylinder, excluding strips
a	=	cylinder diameter
B	=	area of strips
c_0	=	speed of sound
G	=	general Green's function
$G_\pm$	=	Green's functions with specified boundary conditions
I	=	integral, specified by subscript
J_m	=	Bessel function of the first type of order m
k	=	radian frequency/speed of sound
k_r	=	radial wave number
k_x	=	axial wave number
L	=	length of lined section
L_1, L_2	=	linear operators
M_x	=	mean flow Mach number
p_o, p_s	=	incident and scattered pressure fields
p^+, p^-	=	upstream and downstream scattered fields
p_θ	=	azimuthal structure of scattered field
Q	=	bilinear concomitant of operators L_1 and L_2
q	=	integer
r	=	radial distance
S	=	total surface of cylinder
s	=	number of splices
t	=	time
$\boldsymbol{u}$	=	acoustic particle velocity vector
u_r	=	radial component of particle velocity
$\boldsymbol{x}$	=	position vector
x	=	axial distance
Z_A	=	dimensionless impedance of wall lining
Z_B	=	dimensionless impedance of splices
θ	=	azimuthal angle
$\Delta\theta$	=	azimuthal angle spanned by splices
Λ	=	Green's function modal parameter
ρ_0	=	fluid density
χ	=	$[k^2 - (1 - M_x^2)k_r^2]^{1/2}$
ω	=	radian frequency

Received 13 May 2005; revision received 27 February 2006; accepted for publication 13 March 2006.

*Associate Consultant, Institute of Sound and Vibration Research–Fluid Dynamics and Acoustics Group. Senior Member AIAA.

†Research Fellow, Institute of Sound and Vibration Research–Fluid Dynamics and Acoustics Group.

‡Principal Engineer, Noise Engineering. Member AIAA.

§Chief External Research, Noise Engineering, Rolls–Royce plc. Member AIAA.

I. Introduction

IN the drive to reduce the level of noise radiated by modern high-performance aeroengines, it is now common practice to line the intakes and bypass ducts of engines with acoustically absorbent material. Because of constraints in the manufacturing process, and the expense involved, it has been difficult to fit single-piece liner barrels that span the entire circumference of the duct: rather, the liner has usually consisted of several large segments of lining separated by a number of thin longitudinal strips of acoustically hard material. These strips of hard material are referred to as liner splices, and they present a mechanism by which any incident duct mode can scatter energy into a number of other modes. If the scattered modes are more cut-on than the original mode, they will tend to be less well attenuated by the lining, and so the existence of the splices is thus detrimental in terms of the overall attenuation achieved by the liner. Experimental test flights with a Rolls–Royce Tay 650 engine have confirmed that a single-piece liner gives significantly better attenuation than a liner with three longitudinal splices (see [1–3]), and the azimuthal mode scattering effects have been clearly shown in the experimental measurements of Rademaker, Sijtsma, and Tester [4].

Computational aeroacoustic (CAA) methods have been used by various authors [5–9] to model the scattering effects of the splices, but such computational models are generally impractical for use in parametric or liner optimization design studies, because the solution for realistic frequencies of this three-dimensional problem requires a significant amount of CPU time. To overcome this difficulty, we seek to generate an analytical model of the modal scattering by liner splices. Such a model, although facilitating rapid computation in design studies, also leads to a better physical understanding of the problem.

A partial model was derived by Cargill [10] in an internal Rolls–Royce report, and this model was used by Tester, Baker, Kempton and Wright [11] in their study of splice scattering. Using Cargill's methods a complete model is now derived. By Green's function methods an integral expression for the scattered field is derived, and by application of a Kirchhoff approximation this gives the scattered field as an integral over the splice area of an integrand that features only the incident field and a Green's function. This integral is evaluated for a realistic test-case geometry, and the results (for cases both with or without a mean flow) are compared with the results calculated by a CAA code. Good agreement is found between the two sets of results. The CAA code used, ACTRAN, is a finite-element and infinite-element code that assumes linear propagation through an irrotational mean flow. It was developed by Free Field Technologies of Louvain-la-Neuve, Belgium, and has been benchmarked by Astley, Hamilton, Baker, and Kitchen [12] against the analytical solution for radiation from a semi-infinite unflanged duct with uniform mean flow.

In Sec. II of this paper, the general integral expression for the scattered field is derived. In Sec. III the test-case geometry is specified, and a known analytic Green's function is used to calculate the form of the scattered field, then in Sec. IV the analytical predictions are compared with the CAA results.

II. Derivation of General Equation for the Scattered Field

We consider an infinitely long cylindrical duct of radius a, and define a set of cylindrical coordinates $\boldsymbol{x} = (x, r, \theta)$. The inviscid fluid in the duct has density ρ_0 and sound speed c_0, there is a uniform axial mean flow of Mach number M_x in the positive x direction, and the walls are lined with a locally reacting uniform material of impedence Z_A. Arranged on the duct wall are a series of scattering strips, which are flush to the wall but have different Z_B to the rest of the duct. In principle these strips can be arbitrarily arranged within the duct, and need not be of equal length, width or impedance, though in practical situations they are likely to be uniform. Given that a Kirchhoff approximation is to be applied, the area of the strips should be small compared with the duct surface area; $S = A + B$. The acoustic pressure p is decomposed into the sum of two parts, p_O and p_S, where p_O is the field which would be present in the absence of the scattering strips, that is, if the entire duct were of uniform impedance Z_A, and p_S is the scattered field due to the strips. Both of these components of the field are assumed to have harmonic time dependence $e^{i\omega t}$. Then in the linear theory the pressures obey the convected wave equation

$$\left[\nabla^2 - \left(ik + M_x \frac{\partial}{\partial x}\right)^2\right] p_{O,S}(\boldsymbol{x}) = 0 \tag{1}$$

and the linearized momentum equation

$$\rho_0 c_0 \left(ik + M_x \frac{\partial}{\partial x}\right) \boldsymbol{u}(\boldsymbol{x}) = -\nabla p_{O,S}(\boldsymbol{x}) \tag{2}$$

where $\boldsymbol{u}(\boldsymbol{x})$ is the acoustic particle velocity and $k = \omega/c_0$.

The appropriate boundary condition in the presence of a mean flow was first derived for flow along a plane wall by Ingard [13], and later generalized for the case of an arbitrary geometry by Myers [14]. Rienstra [15] has explained the Myers boundary condition in the context of duct acoustics, in terms of a vortex sheet at the duct wall. In the limit of vanishing viscosity, the wall boundary layer becomes a vortex sheet, and the kinematic effect of this sheet must be taken into account when applying the impedance-wall boundary condition. This reduces to the Ingard result for acoustic particle displacement normal to the wall in the case where there is no curvature of the surface in the flow direction. Then the boundary condition for a general pressure p and wall impedance Z is

$$\rho_0 c_0 ik u_r = \left(ik + M_x \frac{\partial}{\partial x}\right)(p/Z) \tag{3}$$

where u_r is the radial component of acoustic particle velocity. Combining Eqs. (2) and (3) gives a boundary condition in terms of p and independent of u_r. By definition, the field p_O is that field which would be present if there were no splices, and so it obeys the boundary condition as if the impedance were Z_A everywhere on the duct wall, and so

$$\frac{(ik + M_x \partial/\partial x)^2}{ik} \left(\frac{p_O(\boldsymbol{x})}{Z_A}\right) = -\frac{\partial}{\partial r} p_O(\boldsymbol{x}) \quad \text{on } S = A + B \tag{4}$$

On the area B of altered impedance, the original and the scattered field must couple in such a way as to satisfy the boundary condition, and so

$$\frac{(ik + M_x \partial/\partial x)^2}{ik} \left(\frac{p_O(\boldsymbol{x}) + p_S(\boldsymbol{x})}{Z_B}\right) = -\frac{\partial}{\partial r} p_O(\boldsymbol{x}) - \frac{\partial}{\partial r} p_S(\boldsymbol{x}) \quad \text{on } B \tag{5}$$

The scattered field must on A satisfy the same boundary condition as the original field:

$$\frac{(ik + M_x \partial/\partial x)^2}{ik} \left(\frac{p_S(\boldsymbol{x})}{Z_A}\right) = -\frac{\partial}{\partial r} p_S(\boldsymbol{x}) \quad \text{on } A \tag{6}$$

The method of solving the above problem is by formulation of an appropriate Green's function superposition integral, which gives the scattered field in the fluid in terms of its values on the surface. A Green's function is defined which satisfies the equation

$$\left[\nabla^2 - \left(ik + M_x \frac{\partial}{\partial x}\right)^2\right] G(\boldsymbol{x}|\boldsymbol{x}_0) = \delta(\boldsymbol{x} - \boldsymbol{x}_0) \tag{7}$$

and boundary conditions to be defined later. The superposition integral is derived by applying a change of variables to Eqs. (1) and (7) to transform them to Helmholtz equations (i.e., eliminating the $\partial/\partial x$ term), multiplying the transformed Eq. (1) by the Green's function and the transformed Eq. (7) by the scattered pressure, subtracting the resulting equations one from the other, integrating the result over the duct volume, applying Green's theorem to change the volume integral to a surface integral, and reverting to the original variables. This type of analysis is well documented, and the details shall not be reproduced here: see, for example, Duffy [16]. The result is

$$p_S(\boldsymbol{x}) = \int_S \left(p_S(\boldsymbol{x}_0) \frac{\partial G(\boldsymbol{x}_0|\boldsymbol{x})}{\partial r_0} - G(\boldsymbol{x}_0|\boldsymbol{x}) \frac{\partial p_S(\boldsymbol{x}_0)}{\partial r_0}\right) \mathrm{d}S_0 \tag{8}$$

where a subscript 0 on an operator implies that the operator acts with respect to the integration variables $\boldsymbol{x}_0$, and r_0 is to be evaluated at a. Note the order of the arguments in the Green's function, and recall that in a mean flow straightforward reciprocity does not apply.

The integral in Eq. (8) is decomposed into the sum of integrals over the two regions A and B, and then the boundary conditions (4–6) are applied in order to replace all terms of the form $\partial p/\partial r_0$ with alternative expressions, giving

$$\begin{aligned} p_S(\boldsymbol{x}) = {} & \int_A \left[p_S(\boldsymbol{x}_0) \frac{\partial G(\boldsymbol{x}_0|\boldsymbol{x})}{\partial r_0} \right. \\ & \left. + G(\boldsymbol{x}_0|\boldsymbol{x}) \frac{(ik + M_x \partial/\partial x_0)^2}{ik} \left(\frac{p_S(\boldsymbol{x}_0)}{Z_A}\right) \right] \mathrm{d}A_0 \\ & + \int_B G(\boldsymbol{x}_0|\boldsymbol{x}) \left[\frac{(ik + M_x \partial/\partial x_0)^2}{ik} \left(\frac{p_O(\boldsymbol{x}_0) + p_S(\boldsymbol{x}_0)}{Z_B}\right) \right. \\ & \left. - \frac{(ik + M_x \partial/\partial x_0)^2}{ik} \left(\frac{p_O(\boldsymbol{x}_0)}{Z_A}\right) \right] \mathrm{d}B_0 \\ & + \int_B \left[p_S(\boldsymbol{x}_0) \frac{\partial G(\boldsymbol{x}_0|\boldsymbol{x})}{\partial r_0} \right] \mathrm{d}B_0 \end{aligned} \tag{9}$$

It is assumed that the impedance of any particular scattering strip is a constant value, or at least not a function of x [the generalization to arbitrary $Z_B(x)$ is discussed later]; the values for different strips can,

however, be different. Then the impedances can be moved to the other side of the differential operators in Eq. (9) as required. Equation (9) contains several terms of the form GL_1p, where L_1 is the linear operator $(ik + M_x\partial/\partial x_0)^2$. It is useful to be able to replace these with terms of the form pL_2G, and from the theory of adjoint operators, it is known that for a certain choice of L_2 this can be done, though an additional term, the bilinear concomitant of the operators, must be taken into account (see, for example, Morse [17], Chaps. 5.2 and 7.5 for a discussion of the bilinear concomitant). The appropriate choice of L_2 is $(ik - M_x\partial/\partial x_0)^2$, and then

$$G(\boldsymbol{x}_0|\boldsymbol{x})L_1p(\boldsymbol{x}_0) - p(\boldsymbol{x}_0)L_2G(\boldsymbol{x}_0|\boldsymbol{x}) = \frac{\partial}{\partial x_0}Q_0[G(\boldsymbol{x}_0|\boldsymbol{x}), p(\boldsymbol{x}_0)] \tag{10}$$

where the bilinear concomitant Q_0 is

$$Q_0[G(\boldsymbol{x}_0|\boldsymbol{x}), p(\boldsymbol{x}_0)] = M_x^2G(\boldsymbol{x}_0|\boldsymbol{x})\frac{\partial p(\boldsymbol{x}_0)}{\partial x_0} - M_x^2p(\boldsymbol{x}_0)\frac{\partial G(\boldsymbol{x}_0|\boldsymbol{x})}{\partial x_0} + 2ikM_xp(\boldsymbol{x}_0)G(\boldsymbol{x}_0|\boldsymbol{x}) \tag{11}$$

No boundary condition for the Green's function has yet been discussed. Although it would be usual to require the Green's function to satisfy a boundary condition similar to the condition (4) for the original pressure field, this is not the condition applied here. Instead, given the change of operators from L_1 to L_2 discussed above, the following condition is applied:

$$\frac{(ik - M_x\partial/\partial x_0)^2}{ik}\left(\frac{G(\boldsymbol{x}_0|\boldsymbol{x})}{Z_A}\right) = -\frac{\partial}{\partial r_0}G(\boldsymbol{x}_0|\boldsymbol{x}) \quad \text{on } S = A + B \tag{12}$$

The Green's function used here is neither the Green's function for the boundary–value problem formulated above, which must obey both the wave Eq. (1) and the Myers boundary condition, nor the reciprocal Green's function, which must obey a mean-flow-reversed reversed wave equation and the reversed boundary condition (12): rather, this Green's function obeys the nonreversed wave Eq. (1) and the reversed boundary condition (12). Label this Green's function as G_-, and the Green's function for the formulated boundary–value problem as G_+. In the following analysis G_- is used, and the change to G_+ is discussed later.

Label the integral over the area A in Eq. (9) as I_A. Then applying the change of operators discussed above to I_A gives

$$\begin{aligned} I_A &= \int_A \left\{ p_S(\boldsymbol{x}_0)\left[\frac{\partial G_-(\boldsymbol{x}_0|\boldsymbol{x})}{\partial r_0} + \frac{(ik - M_x\partial/\partial x_0)^2}{ik}\left(\frac{G_-(\boldsymbol{x}_0|\boldsymbol{x})}{Z_A}\right)\right] \right. \\ &\quad \left. + \frac{1}{ikZ_A}\frac{\partial}{\partial x_0}Q_0[G_-(\boldsymbol{x}_0|\boldsymbol{x}), p_S(\boldsymbol{x}_0)]\right\} \mathrm{d}A_0 \\ &= \int_S \frac{1}{ikZ_A}\frac{\partial}{\partial x_0}Q_0[G_-(\boldsymbol{x}_0|\boldsymbol{x}), p_S(\boldsymbol{x}_0)]\,\mathrm{d}S_0 \\ &\quad - \int_B \frac{1}{ikZ_A}\frac{\partial}{\partial x_0}Q_0[G_-(\boldsymbol{x}_0|\boldsymbol{x}), p_S(\boldsymbol{x}_0)]\,\mathrm{d}B_0 \end{aligned} \tag{13}$$

where the boundary condition (12) has been applied. In the second line of Eq. (13), the integration with respect to x_0 over the duct area S is trivial, and results in $1/ikZ_A$ multiplied by the difference of the bilinear concomitant evaluated at $x_0 = +\infty$ and $x_0 = -\infty$. Because the duct is lined, the pressure and the Green's functions must decay as $x \to \pm\infty$, and thus the integral over the derivative of the bilinear concomitant must be zero. Then I_A is given as an integral over B of the bilinear concomitant. Applying similar analysis to the integral over B in Eq. (9) gives the result

$$\begin{aligned} p_S(\boldsymbol{x}) &= \int_B [p_O(\boldsymbol{x}_0) + p_S(\boldsymbol{x}_0)]\frac{(ik - M_x\partial/\partial x_0)^2}{ik} \\ &\quad \times \left[G(\boldsymbol{x}_0|\boldsymbol{x})\left(\frac{1}{Z_B} - \frac{1}{Z_A}\right)\right]\mathrm{d}B_0 \\ &\quad + \int_B \frac{1}{ik}\left(\frac{1}{Z_B} - \frac{1}{Z_A}\right)\frac{\partial}{\partial x_0}Q_0[G(\boldsymbol{x}_0|\boldsymbol{x}), p_O(\boldsymbol{x}_0) \\ &\quad + p_S(\boldsymbol{x}_0)]\,\mathrm{d}B_0 \end{aligned} \tag{14}$$

If the scattering strips extend to infinity along the duct, the radiation condition dictates that the contribution from the second integral in Eq. (14) is zero. For finite strips, the contribution from the second term goes to zero if M equals zero. The first term describes the basic scattering, which occurs along the length of the strips, whereas the second term describes additional scattering from the ends of the strips, generated by interaction between the axial mean flow and the discontinuity in the axial direction of the boundary conditions. The duct to be modeled later in this paper contains a finite length lined region with splices, and beyond this region the walls are hard: the splices run the entire length of the lined region, and thus the transition in the x direction from lined area to splice does not occur and so the second term in Eq. (14) is not required (whereas the transition from liner to hard wall is best modeled by another method, to be discussed). The second term in Eq. (14) thus only becomes important when the splices are of shorter length than the lined section of duct. The first term in Eq. (14) was originally derived by Cargill [10], in an internal Rolls–Royce report, but he ignored the end effects described by the second term.

In applying Eq. (14), it is useful to be able to use the Green's function G_+ for a lined duct with flow, as derived by Rienstra and Tester [14], and applied by Tester et al [11]. The Green's function G_- used above obeys the reversed boundary condition (12), whereas G_+ obeys the standard Myers' type boundary condition

$$\frac{(ik + M_x\partial/\partial x)^2}{ik}\left(\frac{G_+(\boldsymbol{x}|\boldsymbol{x}_0)}{Z_A}\right) = -\frac{\partial}{\partial r}G_+(\boldsymbol{x}|\boldsymbol{x}_0) \quad \text{on } S = A + B \tag{15}$$

Because both G_+ and G_- obey the convected wave equation, we can derive, by methods identical to those used to derive the superposition integral (8), the equality

$$\begin{aligned} G_+(\boldsymbol{x}_0|\boldsymbol{x}_1) - G_-(\boldsymbol{x}_1|\boldsymbol{x}_0) &= \int_S \left(G_-(\boldsymbol{x}|\boldsymbol{x}_0)\frac{\partial G_+(\boldsymbol{x}|\boldsymbol{x}_1)}{\partial r} \right. \\ &\quad \left. - G_+(\boldsymbol{x}|\boldsymbol{x}_1)\frac{\partial G_-(\boldsymbol{x}|\boldsymbol{x}_0)}{\partial r}\right)\mathrm{d}S \end{aligned} \tag{16}$$

Applying the boundary conditions (12) and (15) to Eq. (16) gives an integral over an expression of the form $G_+L_2(G_-/Z_A) - G_-L_1(G_+/Z_A)$, which, because Z_A is constant, gives

$$G_+(\boldsymbol{x}_0|\boldsymbol{x}_1) - G_-(\boldsymbol{x}_1|\boldsymbol{x}_0) = \int_S \frac{-1}{ikZ_A}\frac{\partial}{\partial x}Q[G_-(\boldsymbol{x}|\boldsymbol{x}_0), G_+(\boldsymbol{x}|\boldsymbol{x}_1)]\,\mathrm{d}S \tag{17}$$

Calculation of the integral with respect to x in Eq. (17) is trivial, and by the radiation condition, assuming a finite impedance along the duct to infinity, the result is zero. (A method for considering hard walls to infinity is noted at the end of this section.) Thus the two Green's functions can be interchanged, so long as the arguments are reversed: this resembles a reciprocity theorem, despite the fact the mean flow is not reversed: it only holds in the special case where Z_A is a constant. If Z_A was a function of x, the interchanging of the operators would not give a bilinear concomitant in the form shown above, and the integration could not necessarily be done, and so the Green's functions could not be interchanged: this stands to reason, because G_+ and G_- must react differently to changes in the surface impedance. For the rest of this report, we apply the change of Green's function to Eq. (14), so that the standard lined-duct Green's function is applied.

A Kirchhoff approximation is now applied: if the scattered field is of small amplitude compared with the original field, then the scattered field can be approximated by carrying out the surface integrals in Eq. (14) using only the original field, that is, we assume $p_O(\boldsymbol{x}) \gg p_S(\boldsymbol{x})$. Furthermore, it is assumed throughout the rest of this report that the scattering strips are acoustically hard, and so $Z_B \to \infty$. Thus the equation for the scattered field is

$$p_S(\boldsymbol{x}) = -\int_B p_O(\boldsymbol{x}_0)\frac{(ik - M_x\partial/\partial x_0)^2}{ikZ_A}G(\boldsymbol{x}|\boldsymbol{x}_0)\,\mathrm{d}B_0 - \int_B \frac{1}{ikZ_A}\frac{\partial}{\partial x_0}Q_0[G(\boldsymbol{x}|\boldsymbol{x}_0), p_O(\boldsymbol{x}_0)]\,\mathrm{d}B_0 \tag{18}$$

Equation (18) is the central result, which shall be applied in the following section of the paper. The first term, derived by Cargill [10], describes scattering along the length of the splice, whereas the second term describes end effects. It is valid for the case of a duct that is lined for its entire length with a uniform material, which contains an arbitrary arrangement of acoustically hard splices. The equation cannot be applied to the case of liners or splices for which the acoustic impedances are functions of the longitudinal coordinate x. This is because the impedance appears in front of the differential operators in the boundary conditions, which implies that when manipulating the operators L_1 and L_2 the resulting bilinear concomitant must be of a more complicated form. Furthermore, as mentioned above, Z_A must be constant to allow the changing of the Green's functions. However, in the analysis of the following section of this paper, we consider a case where the lining makes up only a finite length of an otherwise unlined duct: in this case it is assumed that the above formula can be applied as an approximation inside the lined-duct section, and that appropriate matching conditions must be applied at the ends of the lined-duct section.

III. Application of General Equation to Engine Intake Problem

We consider the application of spliced liners in the inlet duct of an aeroengine. The mean flow is toward the fan, and the fan tone propagates upstream from the fan. The duct section upstream of the fan consists of a short hard-walled section, followed by a lined section with splices, followed by a further hard-walled section before the end of the duct. The geometry is shown in Fig. 1, where the fan plane is labeled x_0, the interface plane between the downstream hard-walled section and the lined section is labeled x_1, the interface between the lined section and the upstream hard-walled section is x_2 and the intake plane is x_3; the length of the lined section is L and the duct radius is a. As the rotor generated mode reaches the interface x_1, some sound is reflected back toward the fan but most propagates into the lined section, where it is then scattered by the splices into a number of modes. The pressure field in the lined section is composed of a backward-scattered and a forward-scattered field, and as the forward-scattered field and the original mode meet the interface x_2,

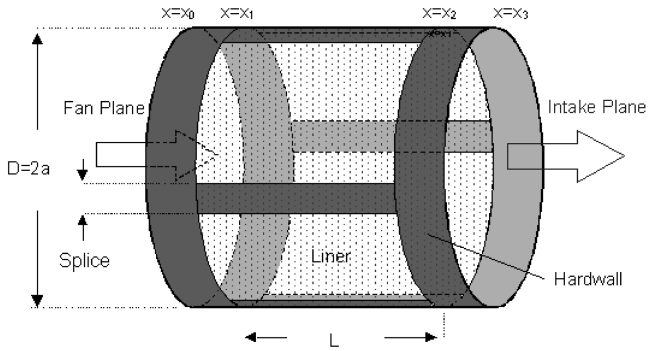

Fig. 1 The geometry of the model duct. Sections A and C are hard walled, and Sec. B is lined and has a number of longitudinal splices present. The incident mode propagates from left to right, and the mean flow is from right to left.

they are again partially reflected and transmitted. The sound power that is transmitted into the upstream hard-walled section will be approximately equal to the sound power radiated from the end of the duct and into the far field. In modeling the propagation of the fan tone forward through the duct, it is assumed that the hard and lined sections can be treated separately, with appropriate matching conditions applied at the interfaces.

Within the lined section, the theory derived above is applied, to calculate the scattering effects of the liner splices. An origin for the coordinate system is chosen such that the lined section extends from $x = -L/2$ to $x = L/2$. The incident pressure at the plane $x = -L/2$ is taken to be the rotor-alone mode, which has azimuthal mode number M and radial mode order 1:

$$p_0(\boldsymbol{x}_0) = p_{M1}J_M(k_{rM1}r_0)e^{-ik_{xM1}(x_0+L/2)}e^{-iM\theta_0} \tag{19}$$

where J_M is the Bessel function of the first type of order M, k_{rM1} is the radial wave number, and k_{xM1} is the axial wave number. Tester et al. [11] have used an analytic, closed form Green's function for a lined duct with a mean flow, which was deduced from that given by Tester [18] for a lined two-dimensional duct containing a uniform flow. This was assumed to be an approximation, though it has been shown that it is a special case of the result derived by Swinbanks [19] for a lined two-dimensional duct containing a sheared flow. The three-dimensional Green's function used by Tester et al. [11] has now been shown to be analytically correct, with the derivation given by Rienstra and Tester [20]. The Green's function is

$$G_+(\boldsymbol{x}|\boldsymbol{x}_0) = \frac{-1}{2\pi i}\sum_{m=-\infty}^{\infty}\sum_{n=1}^{\infty}\frac{J_m(k^{\pm}_{rmn}r)J_m(k^{\pm}_{rmn}r_0)}{a^2\chi^{\pm}_{mn}\Lambda^{\pm}_{mn}}e^{\mp ik^{\pm}_{xmn}(x-x_0)}e^{-im(\theta-\theta_0)} \tag{20}$$

where the upper sign is taken throughout for $x > x_0$, and the lower sign taken for $x < x_0$. For $x > x_0$ the sum over n pertains to rightward propagating waves, whereas for $x < x_0$ the sum over n pertains to leftward propagating waves. We apply a condition that the axial wave numbers $k^{\pm}_{xmn}$ are taken to lie in the lower half of the complex k_x plane, and thus all modes obey the radiation condition (see, for example, Howe [21], Chap. 1). The wave numbers obey the equalities

$$k^{\pm}_{xmn} = (\mp M_x k \pm \chi^{\pm}_{mn})/(1 - M_x^2) \quad \text{and} \quad \chi^{\pm}_{mn} = [k^2 - (1 - M_x^2)k^{\pm 2}_{rmn}]^{1/2} \tag{21}$$

and are determined by the roots of the transcendental equation

$$i(k \mp M_x k_x)^2 J_m(k_r a) + kZ_A k_r J'_m(k_r a) = 0 \tag{22}$$

where a dash denotes differentiation with respect to the argument of the Bessel function. The Λ_{mn} are given as

$$\Lambda^{\pm}_{mn} = J'_m(k^{\pm}_{rmn}a)^2 + J_m(k^{\pm}_{rmn}a)^2\left[1 - \frac{m^2}{k^{\pm 2}_{rmn}a^2} \mp \frac{2iM_x(1 \mp k^{\pm}_{xmn}M_x/k)}{aZ_A\chi^{\pm}_{mn}}\right] \tag{23}$$

Equation (18) describes the scattered sound field in the lined section of the duct. However, in applying this equation we note that the second term, which contains the bilinear concomitant, is not applicable to the present geometry: this term arises due to the discontinuity in the boundary conditions at the end of the splice, but in this case where the splices extend to a hard-walled region, there is no such discontinuity, and the behavior at the interface should be adequately described by the appropriate matching condition that is applied. Thus the scattered field is determined by only the first integral in Eq. (18). We substitute the rotor-alone pressure (19) and the Green's function (20) into the pressure integral, and then divide the axial integral into two parts, which correspond to the forward-scattered and backward-scattered field. These integrals are

$$p^{+}_{mn} = \int_{-L/2}^{x} e^{-ik_{xM1}(x_0+L/2)}(ik - M_x\partial/\partial x_0)^2 e^{-ik^{+}_{xmn}(x-x_0)}\,\mathrm{d}x_0$$
$$= \frac{-i(k - M_x k^{+}_{xmn})^2}{k_{xM1} - k^{+}_{xmn}}\left(e^{-ik_{xM1}(x+L/2)} - e^{-ik^{+}_{xmn}(x+L/2)}\right) \quad (24)$$

and

$$p^{-}_{mn} = \int_{x}^{L/2} e^{-ik_{xM1}(x_0+L/2)}(ik - M_x\partial/\partial x_0)^2 e^{ik^{-}_{xmn}(x-x_0)}\,\mathrm{d}x_0$$
$$= \frac{i(k + M_x k^{-}_{xmn})^2}{k_{xM1} + k^{-}_{xmn}}\left(e^{-ik_{xM1}(x+L/2)} - e^{-ik_{xM1}L}e^{ik^{-}_{xmn}(x-L/2)}\right) \quad (25)$$

The integral with respect to the azimuthal angle is carried out over the number of splices s, where a given splice lies at an angle $\theta_0 = \theta_{0\mu}$ and is of angular width $\Delta\theta_{0\mu}$. The integral is

$$p_{\theta m} = \sum_{\mu=1}^{s}\int_{\theta_{0\mu}}^{\theta_{0\mu}+\Delta\theta_{0\mu}} e^{-im(\theta-\theta_0)}e^{-iM\theta_0}a\,\mathrm{d}\theta_0$$
$$= ae^{-im\theta}\sum_{\mu=1}^{s}\frac{e^{-i(M-m)(\theta_{0\mu}+\Delta\theta_{0\mu})} - e^{-i(M-m)\theta_{0\mu}}}{-i(M-m)} \quad (26)$$

and for the important case of equally spaced splices of equal width, this becomes

$$p_{\theta m} = -sa\Delta\theta\,\mathrm{sinc}(qs\Delta\theta/2)e^{-im\theta} \quad (27)$$

where $\mathrm{sinc}(x) = (1/x)\sin(x)$, q can take any integer value, and m takes only the values

$$m = M + qs \quad (28)$$

This simple relationship means that the number of splices dictates which azimuthal mode orders can be excited by the incident mode.

The complete expression for the scattered field generated by equally spaced splices is

$$p_s(\boldsymbol{x}) = \frac{p_{M1}J_M(k_{rM1}a)}{akZ_A}\sum_{m=-\infty}^{\infty} e^{-im\theta}\left(\frac{sa\Delta\theta}{2\pi a}\right)\mathrm{sinc}(qs\Delta\theta/2)$$
$$\times\sum_{n=1}^{\infty}\left[\frac{J_m(k^{+}_{rmn}r)J_m(k^{+}_{rmn}a)}{\chi^{+}_{mn}\Lambda^{+}_{mn}}p^{+}_{mn} + \frac{J_m(k^{-}_{rmn}r)J_m(k^{-}_{rmn}a)}{\chi^{-}_{mn}\Lambda^{-}_{mn}}p^{-}_{mn}\right] \quad (29)$$

In this expression, the term before the first summation sign is proportional to the amplitude of the scattered mode, and inversely proportional to the impedance of the liner. The first term inside the summation gives the azimuthal mode structure of the generated modes, and the following fraction is then the azimuthal extent of the splices divided by the duct circumference. The sinc function is the fundamental azimuthal scattering function, that determines which azimuthal modes can have energy scattered into them. This function arises from the number of splices present, and is independent of the details of the modal structure. The requirement of integer q selects modes into which energy can be scattered: for example, if the incident mode order is $M = 24$ and there are 2 splices, then energy can only be scattered into even-numbered azimuthal modes. Further, the form of the sinc function determines which of those modes are likely to receive an appreciable fraction of the scattered energy: for values of q large compared with $(s\Delta\theta)^{-1}$ the decay of the function means the scattered amplitude should be small. If the splices are not evenly spaced, the sinc function is replaced by the more general form of the azimuthal scattering function $p_{\theta m}$ given by Eq. (26). The final two terms in the pressure expression (29) are readily interpreted as the forward-scattered and backward-scattered fields, respectively, and include the radial structure of the duct modes.

The above expression for the pressure in the lined region is matched to the hard-walled solutions using the matching conditions of Astley,[‖] which are as yet unpublished. A conventional matching of the solutions across the boundary between the lined and hard-walled sections of duct would involve matching of the pressure and the normal velocity, but Astley has shown that in the presence of mean flow such a matching would be incorrect: the momentum and continuity equations can be used to derive the appropriate matching conditions, which include extra terms. The matching conditions are given in the Appendix, and it can be shown that in the absence of mean flow they reduce to the appropriate conventional matching conditions.

IV. Comparison Between Analytical Results and CAA (ACTRAN) Calculations

In this section, we use numerical solutions from the CAA code ACTRAN to verify the validity of the Cargill method for realistic combinations of parameters. ACTRAN is a commercially available package, based on the finite-element method and the infinite-element method, which assumes irrotational flow and linear propagation. We are using this commercially available code because it is widely used in the aerospace industry, it has been benchmarked against a number of different analytic solutions, and it is a flexible, robust, well-supported code. We will not therefore attempt to justify the solution method here or the pre- and postprocessing available within this code, for example, the quality of its nonreflecting boundary conditions, how it handles the modal excitation of a given system or how it extracts modal information from the numerical solution. This information is largely available to would be, or actual, users of the code.

However, we should emphasize that the ACTRAN code has been designed such that the acoustic excitation can be specified in terms of incoming duct modes, and the nonreflecting boundary conditions have been found to be most effective.

Details of the finite-element mesh used for the ACTRAN calculations are as follows. The finite-element mesh is unstructured across the y–z plane, with two elements allocated azimuthally for each splice at the wall. In the main, quadrangular elements have been used with just a few triangular elements in the vicinity of the splice. The maximum mesh size is $\sim 0.02a$. The unstructured mesh is extruded axially to form a structured mesh in the axial direction comprising hexahedral or pentahedral elements with a nominal axial length of $0.02a$ but this is reduced near the hard/lined interface to $0.01a$. These features are shown in Figs. 2–4.

It is beyond the scope of this paper to investigate the details of how the ACTRAN solutions behave in the vicinity of the hard wall to lined wall interface, especially in the presence of mean flow, but we need to demonstrate that the ACTRAN solutions are essentially valid in terms of the axial sound power, which is the parameter that we use here as the basis for the verification of the Cargill solutions. This means that we have to conduct some elementary verification of the numerical solutions but for a simpler configuration, which admits an analytic solution, using the same mesh. For this we choose the case that is identical to the present problem except there are no splices present. We construct a solution from the standard analytic eigenfunctions for a uniformly lined duct and a hard wall duct and use mode matching at the hard-lined interfaces. Thus we obtain these analytic solutions, for no flow and with uniform flow and also the corresponding ACTRAN solutions for the case where we have completely uniform liner of the same length bounded with the same hard wall sections at each end, as in Fig. 1.

The comparisons are given in Fig. 5 for no flow and in Fig. 6 for the flow case (acoustic and flow parameter details are given below), showing that in terms of the axial sound power of a single azimuthal mode, the analytic and ACTRAN solutions are virtually indistinguishable for the uniform liner case. The ACTRAN results in Figs. 5 and 6 have been calculated by first decomposing the numerical solution for the pressure and axial particle velocity at each point in the mesh into azimuthal Fourier components (at a number of radial and axial positions), and then calculating the axial intensity using the Morfey [22] definition. We have computed the sound power crossing each axial plane by integrating the axial intensity

[‖]Astley, R. J., private communication, Southampton University, 2005.

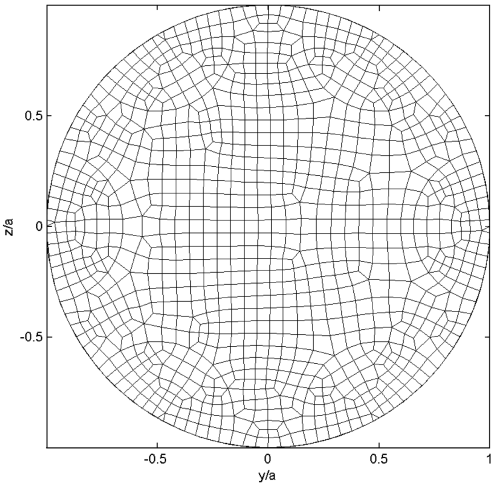

Fig. 2 View of mesh used for ACTRAN calculations showing unstructured mesh in y–z plane, which is extruded in the axial direction (x).

with respect to area. The ACTRAN code also provides some more detailed quantities, namely the sound power in each azimuthal/radial mode, separated into upstream and downstream values, *but only at the duct entry and duct exit,* that is, at $x/a = -0.3$ and $x/a = 0.3$. We compare these ACTRAN values (which when summed agree with the values plotted in Figs. 5 and 6 at the inflow and outflow) with the analytic values in Table 1 below. It can be seen that the agreement is to within 0.1 dB for the zero flow case and to within 0.4 dB for the flow case. We can therefore assume that for all practical purposes the mesh is adequate for the present study.

We now consider the case when splices are introduced into the otherwise uniform liner. The incident rotor-alone mode has azimuthal wave number $M = 24$, with a cut-on ratio of 1.1, where the cut-on ratio is defined as $ka/[k_r a(1 - M_x^2)^{1/2}]$. This choice of cut-on ratio corresponds to the cutback noise certification condition on modern bypass engines where splice scattering has been observed to be most significant. Higher values of cut-on ratio are of less interest, because the rotor-alone decay rapidly reduces with increasing cut-on ratio, so that the splice scattered modes become unimportant relative to the rotor mode. The fixed cut-on ratio causes ka (the product of wave number and duct radius) to vary depending on the presence or absence of a mean flow. The dimensionless impedance Z_A takes the complex value $2–i$. The duct radius a is 127 cm, the length of the lined region is $L = 0.48a$, and there are six evenly spaced splices each of 7.62 cm in width. Then $s\Delta\theta$ is small, and from the sinc function in Eq. (29) it is expected that significant energy will be scattered into a significant number of azimuthal modes: however, any generated modes with higher mode numbers than the rotor-alone mode are cut off, and do not propagate through the lined region, so that in the following figures we look only at modes with lower mode numbers than the incident mode. The figures show the axial variation of the sound power level in dB (PWL) (as defined by Morfey [22]) per mode normalized by the sound power level of the incident mode. Levels are shown for the rotor-alone mode and the four cut-on scattered modes with $m \geq 0$, and the total PWL calculated using all of the scattered modes. The power in each mode has been calculated by performing a Fourier decomposition of the pressure and axial particle velocity with respect to azimuthal angle over each axial plane in the mesh. First, the case

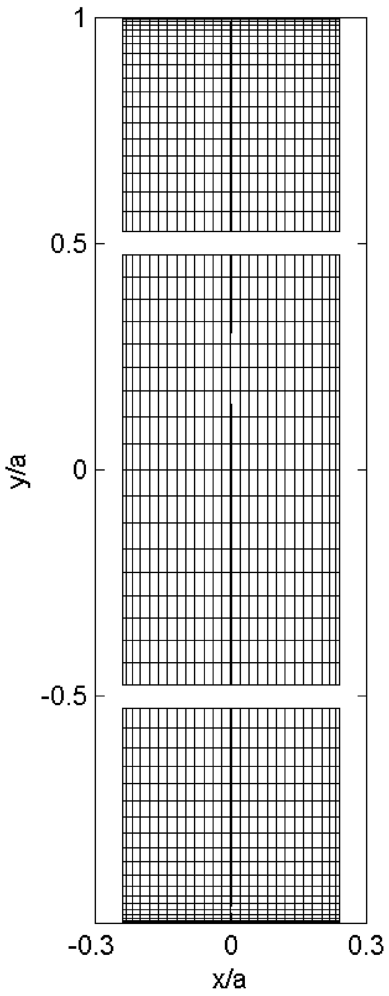

Fig. 3 View of mesh used for ACTRAN calculations showing 1) structured surface mesh elements in acoustic liner, 2) splices shown in white.

with no mean flow is considered, and then the case with a mean flow is treated.

Figures 7 and 8 show the results for the no-flow case, with Fig. 7 showing the ACTRAN calculation, and Fig. 8 showing the Cargill result. In this case $ka = 29$. The two sets of results agree well, except for some discrepancies near the interface between the lined and hard-walled sections at x1, where the backscattered modes dominate the field. In this region the net sound power changes direction from downstream to upstream, leading to the sharp minima in the PWL of the scattered modes. The predicted amplitude of the backscattered modes differs from ACTRAN by about 2 dB. However, in the more important case of the forward-scattered modes, the Cargill prediction agrees very well with the ACTRAN calculation. A striking feature of the results is that most of the forward-scattered modes are of almost equal sound power level, with none of them being strongly attenuated by the liner. In this particular example the effect of the presence of the splices is to reduce the efficiency of the liner by about 5 dB.

Figures 9 and 10 show the results for the more important case where the parameter values are the same as above except we have a

Table 1 Comparison of ACTRAN and analytic results for axial reflected power and axial transmitted power, relative to incident power in rotor-alone mode $m = 24$, uniform liner (no splices)

M_x	Azimuthal mode	PWL reflected at $x = -0.3$		PWL transmitted at $x = +0.3$	
		Analytic	ACTRAN	Analytic	ACTRAN
0	24	−13.3	−13.3	−29.4	−29.3
−0.4	24	−11.6	−11.4	−46.4	−46.8

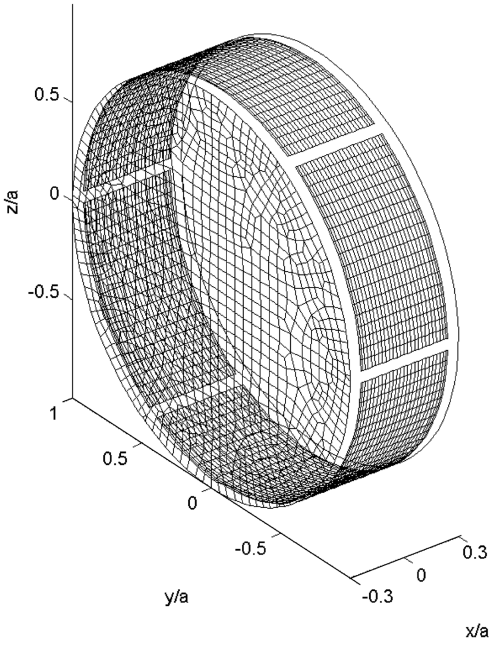

Fig. 4 View of mesh used for ACTRAN calculations showing unstructured transverse mesh and structured surface mesh elements in acoustic liner, hard surfaces and hard splices shown in white.

mean flow of Mach number $M_x = -0.4$, and $ka = 26.57$: Fig. 9 shows the ACTRAN calculation and Fig. 10 shows the Cargill result, with the Astley matching conditions applied. We again see some minor inaccuracies in the backscattered modes, but generally the agreement between the two sets of results is good. In this case the sound power of most of the generated modes exceeds that of the rotor-alone mode at the upstream end of the duct, as they are very poorly attenuated by the liner, and so the overall effect of the liner splices in this case is to reduce the efficiency of the liner by over 20 dB.

With regard to the backscattered mode power levels between the duct entry at $x/a = -0.3$ and the start of the lined section at $x/a = -0.24$, the Cargill results in Figs. 8 and 10 show no variation with x, which is as it should be, whereas the ACTRAN results in Figs. 7 and 9 do show some variation, particularly for the flow case in Fig. 9. This indicates that the mesh is beginning to fall short of the required resolution. However variations elsewhere and especially in the forward-scattered mode power levels between $x/a = 0.24$ at the end of the lined section and $x/a = 0.3$ are less than 1 dB, which is where accurate results are required.

To confirm the accuracy of the Cargill results for the forward-scattered mode power levels, Table 2 compares the Cargill and ACTRAN modal power results for the no-flow and the flow cases at the duct exit, showing that the agreement is indeed better than 1 dB.

The verification of the Cargill model with ACTRAN solutions has been limited to one combination of frequency and liner impedance and strictly speaking more work is needed to determine the limits of applicability of the Cargill model in terms of those key parameters. However, the values used here are typical of those encountered in engine intake liners and it is unlikely that we will encounter any serious limitations on the frequency parameter. The impedance range is more of an issue, because the Cargill result predicts the scattering to be inversely proportional to the impedance and hence small impedance values can therefore be a problem. Cargill [10] provided some guidance on how to deal with this by using a slightly different expression, and this will be the subject of future investigation.

V. Conclusion

An analytical model for the scattering of sound by liner splices has been developed, and its predictions have been shown to agree well with those obtained from a commercially available CAA code, for a physically relevant set of parameters. The analytical model helps to

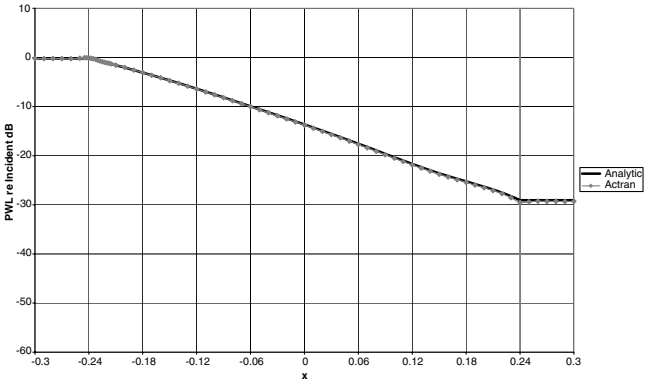

Fig. 5 Analytical and ACTRAN results for a no-flow case, no splices.

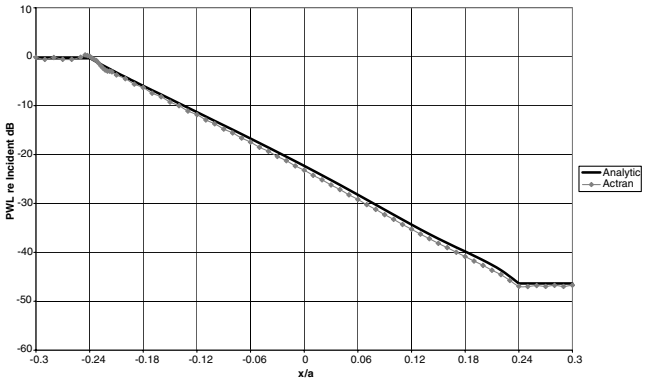

Fig. 6 Analytical and ACTRAN results for a uniform flow case, with $M_x = -0.4$, no splices.

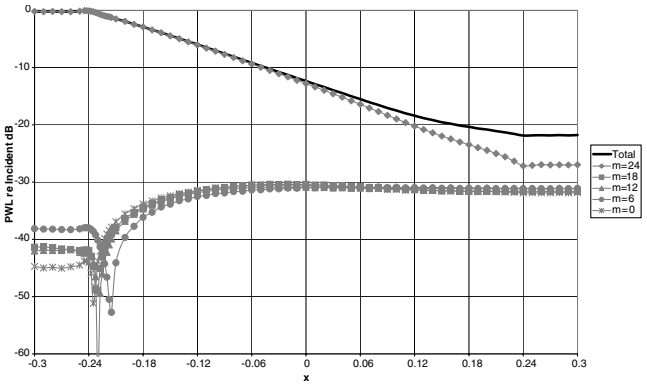

Fig. 7 ACTRAN results for no-flow case.

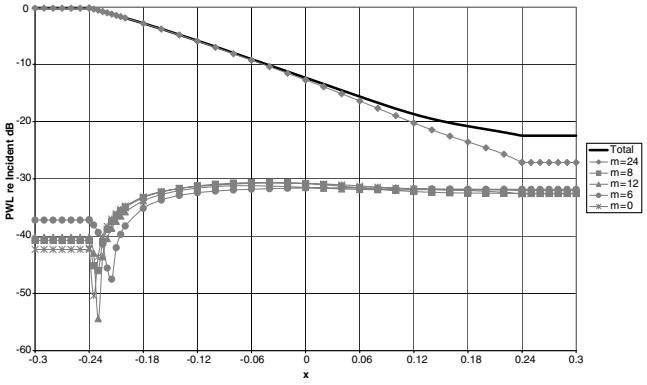

Fig. 8 Cargill results for no-flow case.

Table 2 Comparison of ACTRAN and Cargill results for axial transmitted sound power level, relative to incident power level, in rotor-alone mode $m = 24$ and splice scattered modes

Azimuthal mode	PWL transmitted at $x = +0.3$ $Mx = 0$			PWL transmitted $x = +0.3$ $Mx = -0.4$		
	Cargill	ACTRAN	Delta	Cargill	ACTRAN	Delta
24	−27.2	−27.0	0.2	−46.2	−46.4	−0.2
18	−32.5	−31.6	0.9	−32.9	−33.0	−0.1
12	−32.0	−31.1	0.9	−31.8	−32.2	−0.6
6	−31.8	−31.1	0.7	−31.0	−31.7	−0.7
0	−32.6	−31.8	0.8	−31.5	−32.0	−0.5

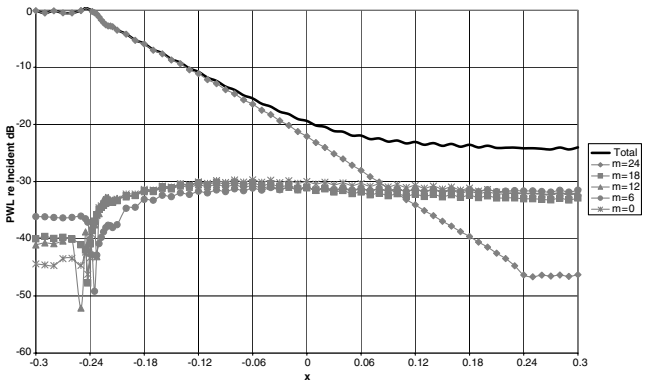

Fig. 9 ACTRAN results for a uniform flow case, with $M_x = -0.4$.

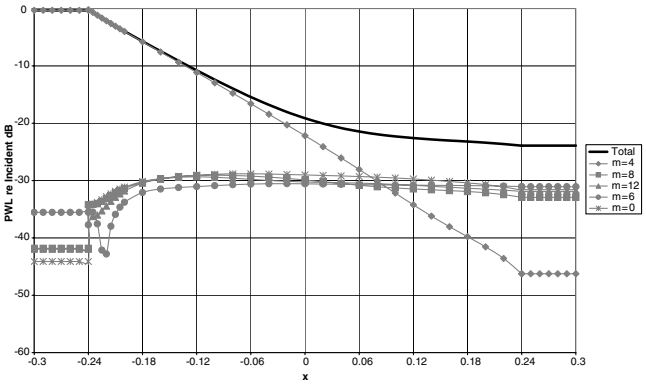

Fig. 10 Cargill results for a uniform flow case, with $M_x = -0.4$.

improve our understanding of the scattering process, and provides a very rapid method of calculating splice scattering effects. With the aid of CAA solutions such as those shown above, the limits of the model are being explored in terms of key parameters such as Helmholtz number, Mach number and liner impedance, and more general splice arrangements are being investigated, for which the end effects described by the bilinear concomitant contributions may become important.

Appendix

R. J. Astley, of the University of Southampton, has derived a set of matching conditions for the problem of a sound field in a duct with an axial discontinuity in the wall impedance, which take account of the effects of a mean flow.

Consider a duct that has wall impedance Z_I to the left of the plane $x = 0$, and Z_{II} to the right of this plane, so that there is a discontinuity in the boundary conditions at $x = 0$. Let the pressure and particle velocity to the left of this plane be p_I and $\boldsymbol{u}_I$, and those to the right be p_{II} and $\boldsymbol{u}_{II}$, and let the mean flow be U_0 and the mean density ρ_0. Let S^+ and S^- be surfaces of fixed x that span the duct width and lie at limiting values $x = 0^+$ and $x = 0^-$, and similarly let C^+ and C^- be the lines of intersection between the surfaces S^+ and S^- and the duct surface. Then the matching conditions are

$$U_0 \int_{S-} W\boldsymbol{u}_I \cdot \boldsymbol{e}_x \,\mathrm{d}S + \frac{1}{\rho_0}\int_{S-} W p_I \,\mathrm{d}S = U_0 \int_{S+} W\boldsymbol{u}_{II} \cdot \boldsymbol{e}_x \,\mathrm{d}S + \frac{1}{\rho_0}\int_{S+} W p_{II} \,\mathrm{d}S \tag{A1}$$

and

$$\int_{S-} W(U_0 p_I + \rho_0 c_0^2 \boldsymbol{u}_I \cdot \boldsymbol{e}_x)\,\mathrm{d}S - \frac{iU_0}{k}\int_{C-} \frac{W p_I}{Z_{\mathrm{I}}}\,\mathrm{d}C = \int_{S+} W(U_0 p_{II} + \rho_0 c_0^2 \boldsymbol{u}_{II} \cdot \boldsymbol{e}_x)\,\mathrm{d}S - \frac{iU_0}{k}\int_{C+} \frac{W p_{\mathrm{II}}}{Z_{II}}\,\mathrm{d}C \tag{A2}$$

where W is an appropriate weighting function [e.g., $J_m(k_r r)\exp(-im\theta)$] and $\boldsymbol{e}_x$ is a unit vector in the axial direction. If the mean flow U_0 goes to zero, these reduce to standard matching of pressure and axial velocity. The implementation of the matching conditions is discussed in Astley et al [23].

Acknowledgments

The authors would like to acknowledge the contributions of the late Alex M. Cargill, who originally formulated the basic model used in this work. The authors would also like to acknowledge the help and advice of Matthew Wright and Jeremy Astley who pioneered the work on splice modeling with the ACTRAN code at the ISVR; also our thanks to James Hamilton who generated the meshes used in these calculations.

References

[1] Sarin, S. L., and Rademaker, E. R., "In-Flight Acoustic Mode Measurements in the Turbofan Engine Inlet of Fokker 100 Aircraft," AIAA Paper 93-4414, 1993.

[2] Henshaw, D. G., "Aeroacoustics Methods for Fan Noise Prediction and Control," Rolls–Royce, FAN-PAC Final Technical Rept. FANPAC-RR-96-9.1, Derby, U.K., Aug. 1996.

[3] Rademaker, E. R., Sarin, S. L., and Parente, C. A., "Experimental Investigation on the Influence of Liner Non-Uniformities on Prevailing Modes," AIAA Paper 96-1682, 1996.

[4] Rademaker, E. R., Sijtsma, P., and Tester, B. J., "Mode Detection with an Optimized Array in a Model Turbofan Engine Intake at Varying Shaft Speeds," AIAA Paper 2001-2181, 2001.

[5] Bréard, C., Sayma, A., Imregun, M., and Tester, B. J., "A CFD-Based Non-Linear Model for the Prediction of Tone Noise in Lined Ducts," AIAA Paper 2001-2181, 2001.

[6] Elnady, T., and Boden, H., "Hard Strips in Lined Ducts," AIAA Paper 2002-2444, 2002.

[7] McAlpine, A., and Wright, M., "Finite/Boundary Element Assessment of a Turbofan Spliced Intake Liner at Supersonic Fan Operating Conditions," AIAA Paper 2003-3305, 2003.

[8] Regan, B., and Eaton, J., "Modelling the Influence of Acoustic Liner Non-Uniformities on Duct Modes," *Journal of Sound and Vibration*, Vol. 219, No. 5, 1999, pp. 859–879.

[9] Di Francescantonio, P., Casalino,D., and De Mercato, L., "Aeroacoustic Design of Aero-Engine Intake Liners," AIAA Paper 2005-2942, 2005.

[10] Cargill, A. M., "Scattering from Joins Between Liners in Intake Ducts with Application to BR710 Buzz-Saw Noise," Rolls–Royce, Rept. TSG0688, Derby, U.K., June 1993.

[11] Tester, B. J., Baker, N. J., Kempton, A. J., and Wright, M. C., "Validation of an Analytical Model for Scattering by Intake Liner

Splices," AIAA Paper 2004-2906, 2004.
[12] Astley, R. J., Hamilton, J. A., Baker, N., and Kitchen, E. H., "Modelling Tone Propagation from Turbofan Inlets—the Effect of Extended Lip Liners," AIAA Paper 2002-2449, 2002.
[13] Ingard, K. U., "Influence of Fluid Motion Past a Plane Boundary on Sound Reflection, Absorption and Transmission," *Journal of the Acoustical Society of America*, Vol. 31, No. 7, 1959, pp. 1035–1036.
[14] Myers, M. K., "On the Acoustic Boundary Condition in the Presence of Flow," *Journal of Sound and Vibration*, Vol. 71, No. 3, 1980, pp. 429–434.
[15] Rienstra, S. W., "A Classification of Duct Modes Based on Surface Waves," *Wave Motion*, Vol. 37, 2003, pp. 119–135.
[16] Duffy, D. G., *Green's Functions with Applications*, 1st ed., Chapman and Hall/CRC, Boca Raton, 2001.
[17] Morse, P. M., and Feshbach, H., *Methods of Theoretical Physics*, 1st ed., McGraw–Hill Book Company, New York, 1953.
[18] Tester, B. J., "The Propagation and Attenuation of Sound in Ducts Containing Uniform or 'Plug' Flow," *Journal of Sound and Vibration*, Vol. 28, No. 2, 1973, pp. 151–203.
[19] Swinbanks, M. A., "The Sound Field Generated by a Source Distribution in a Long Duct Carrying Sheared Flow," *Journal of Sound and Vibration*, Vol. 40, No. 1, 1975, pp. 51–76.
[20] Rienstra, S. W., and Tester, B., "An Analytic Green's Function for a Lined Circular Duct Containing Uniform Mean Flow," *11th AIAA/CEAS Aeroacoustics Conference*, 2005 (to be published).
[21] Howe, M. S., *Acoustics of Fluid Structure Interactions*, 1st ed., Cambridge University Press, Cambridge, U.K., 1998.
[22] Morfey, C. L., "Acoustic Energy in Non-Uniform Flows," *Journal of Sound and Vibration*, Vol. 14, No. 2, 1971, pp. 159–170.
[23] Astley, R. J., Hii, V., and Gabard, G., "A Computational Mode-Matching Approach for Propagation in Three-Dimensional Ducts with Flow," AIAA Paper 2006-2528, 2006.

C. Bailly
Associate Editor